LONGITUDINAL AND SPANWISE STRUCTURES IN A TURBULENT WAKE

H.J. Zhang[1], Y. Zhou[1], R.A. Antonia[2]
[1]Department of Mechanical Engineering
The Hong Kong Polytechnic University
Hung Hom, Kowloon, Hong Kong
[2]Department of Mechanical Engineering
University of Newcastle, N.S.W., 2308, Australia

ABSTRACT

Approximations to the three vorticity components ω_x, ω_y and ω_z have been simultaneously obtained using a combination of four X-wires in the near-wake of a circular cylinder. The present objective is to investigate the likely spatial relationship between longitudinal and spanwise vortical structures. Conditional distributions of ω_x and ω_y, based on detections of spanwise structures, indicated that the longitudinal structures are located upstream of the saddle point. The angles of the vorticity vector suggest that the most likely inclination, to the x-axis, of longitudinal structures is about 50°, aligned with the diverging separatrix between two consecutive spanwise structures. About 40% of $\overline{\omega_x^2}$ and $\overline{\omega_y^2}$ occur within the spanwise vortical structures, apparently resulting from the three-dimensionality of the structures, while the non-vortical regions account for 60%, which is largely attributed to the longitudinal structures. Spanwise structures also account for about 60-80% of $\overline{\omega_z^2}$.

1. INTRODUCTION

Previous research on the turbulent near-wake has revealed two main types of vortical structures, which contribute to the three-dimensionality of this flow. One is the quasi-two-dimensional spanwise structure with predominantly spanwise vorticity (Hussain & Hayakawa 1987; Zhou & Antonia 1993). The other is the longitudinal structure. It generally lies in the (x, y)-plane (see Fig. 1 for the definition of the co-ordinate system) and has vorticity components in the x- and y-directions only. The latter structure has been suggested to be in the form of ribs (e.g. Kiya & Matrsmura 1988; Hayakawa & Hussain 1989) which either wrap around or connect successive spanwise structures. The presence of ribs has been confirmed at low Reynolds numbers by flow visualisations in near wakes (Meiburg & Lasheras 1987; Williamson 1988; Wu et al. 1994). Using hot-wire data, Zhou & Antonia (1994) provided further evidence of the existence of rib structures at high Reynolds numbers. However, many aspects of ribs remain speculative, including the dynamical role and the spatial relationship between ribs and spanwise structures. This forms the motivation and the major objective of the present work.

Vorticity is an important characteristic of turbulence. The vortical structures are characterised by large-scale vorticity concentrations. Hussain & Hayakawa (1987) advocated that vorticity is the least ambiguous quantity to represent organised structures. However, an accurate measurement of vorticity requires a reliable estimation of velocity gradients. This has proven difficult; the data are scarce, especially of simultaneous measurement of all the three components. Using a combination of four X-wires, Bisset et al. (1990) measured all three components of vorticity in the far-wake of a slightly heated cylinder. One drawback of this approach is that since vorticity is indirectly computed from velocity signals using the central difference approximation, the spacing between X-wires may degrade the spatial resolution of vorticity. This degradation is worse at the higher Reynolds number since the Kolmogrov length scale should decrease when Re_d increases (e.g. Antonia et al. 1996a). Balint et al. (1989, 1991) used a nine-sensor hot-wire probe to measure the three components of vorticity in a mixing layer and a boundary layer respectively. Similar attempts have been made by Tsinober et al. (1992) in grid and boundary layer flows, and by Lemonis (1995) in grid and boundary layer flows. Marasli et al. (1993) measured, with a twelve sensor hot-wire probe, the three components of vorticity in a circular cylinder wake (x/d = 30, where x is the streamwise distance downstream of the cylinder and d is the diameter of cylinder). The present investigation used an approach similar to Bisset et al. (1990) to obtain approximations to the three vorticity components. Although the approach suffers from a degradation in the spatial resolution, it is relatively easy to implement and should be adequate for resolving relatively large-scale vorticity. Since longitudinal structures are expected to have intermediate scales, not drastically different from those of the spanwise structures (Hayakawa & Hussain, 1989), the approach is likely to provide useful qualitative information on both streamwise structures and spanwise structures. Results are presented for root mean square (rms) values of the three vorticity components, spectra, angles of the vorticity vector, conditional vorticity based on the detections of spanwise structures, and contributions from vortical and non-vortical regions to the vorticity variance.

2. EXPERIMENTAL ARRANGEMENT

Experiments were carried out in an open return low turbulence wind tunnel with a 2.4 m long working section (0.35 m × 0.35 m). The bottom wall was tilted to achieve a zero streamwise pressure gradient. A circular cylinder (d = 12.6

mm) was installed in the mid-plane and spanned the full width of the working section, 0.20 m from the exit plane of the contraction. This resulted in a blockage of about 3.6% and an aspect ratio of 27.6. Measurements were made at x/d = 20 and Re ($\equiv U_\infty d/\nu$, where U_∞ is the free stream velocity and ν the kinematic viscosity) = 5600. The free stream longitudinal turbulence intensity was about 0.05% and 0.08% respectively; the difference is expected to be within the experimental uncertainty.

Two orthogonal arrays, each of eight X-wires (Figure 1), were used. Four X-wires, i.e. X-wires y1, y2, z4 and z5, were arranged in a manner similar to that of Bisset et al. (1990). They essentially formed a 'vorticity probe', which simultaneously yields approximations to three (large-scale) components of vorticity. X-wires y1 and y2 were parallel to the (x, z)-plane (please refer to Fig 1). The spacing between y1 and y2 are 3.45 mm. X-wires z4 and z5, with a spacing of 4.9 mm, were parallel to the (x, y)-plane, i.e. the plane of mean shear. Six other X-wires were aligned in the (x, y) plane, and six in the (x, z) plane. The sixteen X-wires allow velocity data to be obtained simultaneously. The nominal spacing between X-wires in both planes was about 5 mm. The Kolmogrov length scale η was estimated to be about 0.16mm. All wires were mounted on a frame that was traversed in the y-direction. The physical blockage caused by these arrays, cables and supports was estimated to be about 3%. Several types of measurements (Zhou & Antonia, 1994) indicated that the interference to the flow due to the two arrays was negligible.

Wollaston (Pt-10% Rh) wires, 5 μm in diameter and with an active length of about 1 mm, were operated with constant temperature circuits. Signals from the circuits were offset, amplified and then digitized using two 16 channel (12bit) A/D boards and two personal computers at a sampling frequency f_s = 3.5 kHz per channel. The acquisition of the data by the two computers was synchronized using a common external trigger pulse. The wires were calibrated for velocity and yaw, and continuously checked for drift. Using velocity and yaw calibrations,

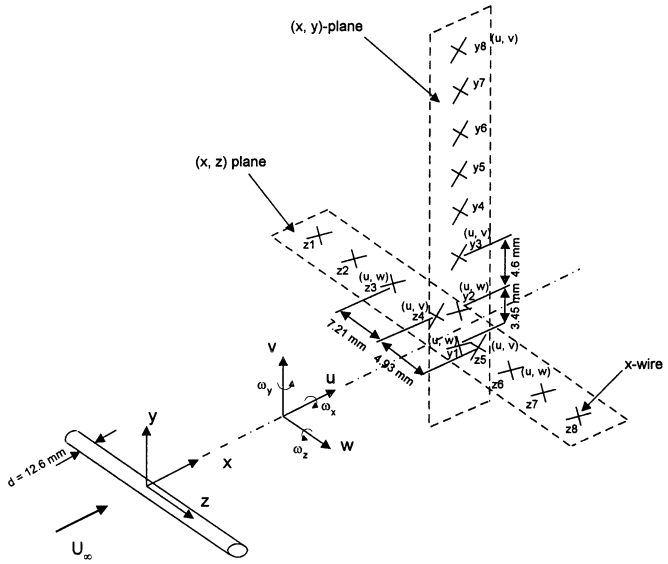

Figure 1 Experimental arrangement

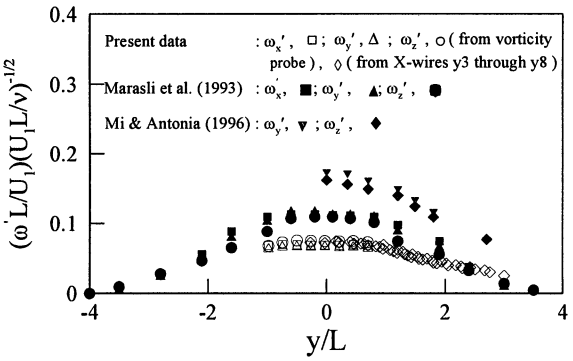

Figure 2 Lateral distributions of $(\omega' L/U_1)(U_1L/\nu)^{-1/2}$

signals proportional to velocity fluctuations *u*, *v* and *w*, together with the local mean velocities $\overline{U}$, $\overline{V}$ (≈ 0) and $\overline{W}$ (≈ 0), were formed on digital tape. The duration of each record was about 38s.

3. APPROXIMATION OF VORTICITY COMPONENTS

The vorticity components are defined in terms of the derivatives of the instantaneous velocities $U = \overline{U} + u$, $V \approx v$ ($\overline{V} \approx 0$) and $W \approx w$ ($\overline{W} \approx 0$), where an overbar denotes time averaging. Since $\partial\overline{U}/\partial z$ is zero, large-scale approximations to the three components of vorticity at the centre of X-wires y1, y2, z4 and z5 are

$$\omega_x = \frac{\partial W}{\partial y} - \frac{\partial V}{\partial z} = \frac{\partial w}{\partial y} - \frac{\partial v}{\partial z} \approx \frac{\Delta w}{\Delta y} - \frac{\Delta v}{\Delta z} \quad (1a)$$

$$\omega_y = \frac{\partial U}{\partial z} - \frac{\partial W}{\partial x} = \frac{\partial u}{\partial z} - \frac{\partial w}{\partial x} \approx \frac{\Delta u}{\Delta z} - \frac{\Delta w}{\Delta x} \quad (1b)$$

$$\omega_z = \frac{\partial V}{\partial x} - \frac{\partial U}{\partial y} = \frac{\partial v}{\partial x} - \frac{\partial(\overline{U}+u)}{\partial y} \approx \frac{\Delta v}{\Delta x} - \frac{\Delta(\overline{U}+u)}{\Delta y} \quad (1c)$$

In computing vorticity, central finite differences between the two points on either side of the probe centre, in both z and y directions, were used. In Eq (1), Δy (= 3.45 mm) and Δz (= 4.9 mm) are spacings between X-wires y1 and y2, z4 and z5, respectively; $\Delta x = -U_c \Delta t$, where $\Delta t = 1/f_s$ and $U_c = 0.87U_\infty$ (Zhou & Antonia 1992) is the average convection velocity. The two derivatives with respect to x are given by

$$\frac{\Delta v}{\Delta x} \approx -\frac{1}{U_c}\frac{\Delta v_0}{\Delta t} \quad (2a)$$

$$\frac{\Delta w}{\Delta x} \approx -\frac{1}{U_c}\frac{\Delta w_0}{\Delta t} \quad (2b)$$

where v_0 and w_0 are the means of the two *v*-values from X-wires z4 and z5, and the two *w*-values from y1 and y2, respectively. The central difference approximation was also used so that the six X-wires, y3 through y8, yielded the instantaneous vorticity at each of the five midpoints between adjacent X-wires (e.g. Zhou & Antonia 1993).

4. RMS DISTRIBUTION AND SPECTRA

The rms values of ω_x, ω_y and ω_z are shown in Fig 2. Note that vorticity is normalised by multiplying it with the factor $(U_1L/\nu)^{-1/2}(L/U_1)$. Antonia et al. (1996a) found that in self-preserving turbulent wall flows, vorticity in the outer region scaled with $(U_\tau\delta/\nu)^{-1/2}(\delta/U_\tau)$, where U_τ is the friction velocity and δ is the boundary layer thickness or half-channel width.

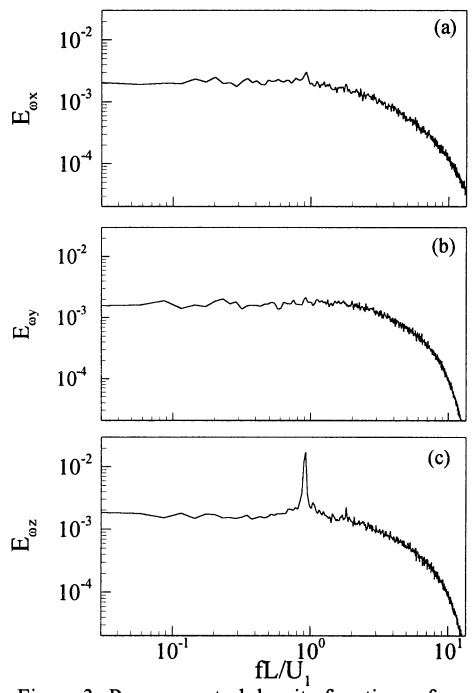

Figure 3 Power spectral density functions of vorticity: (a) streamwise component ω_x, (b) lateral component ω_y, (c) spanwise component ω_z. (y/L ≈ 0.5)

With U_τ and δ replaced by U_1 and L respectively, this scaling was extended to free shear flows, such as jets and wakes. Sreenivasan (1995) also used this scaling for a plane wake. The rms values of ω_z from the 'vorticity probe' agree well with those from X-wires y3 through y8, thus providing a validation of the vorticity data from the present spatial arrangement of X-wires. The present vorticity rms values are lower than those of Marasli et al. (1993, Re=2000) and Mi & Antonia (1996, Re=3000). Marasli et al. used a twelve sensor vorticity probe with a spatial resolution of about 2 mm, while Mi & Antonia used two X-wires, which were separated by 1.2 mm, to measure vorticity. It is likely that the poor spatial resolution of the present data is responsible for the relatively low rms vorticity. Figure 2 indicates that the rms values of the three vorticity components are approximately the same.

Figure 3 presents the power spectral density functions $E_{\omega x}$, $E_{\omega y}$, and $E_{\omega z}$ of ω_x, ω_y, and ω_z at nominally the same point. As expected, $E_{\omega z}$ exhibits a strong peak at the shedding frequency f_s = 106 Hz, *or* $f_s d/U_\infty$ = 0.20, apparently as a result of the occurrence of pseudo-periodic spanwise vortices. Interestingly, a weaker peak is also identifiable in $E_{\omega x}$ at $f_s d/U_\infty$ = 0.20, but is absent in $E_{\omega y}$. It has been suggested (Hussain & Hayakawa, 1987; Zhou & Antonia, 1994) that the rib structure is located between successive spanwise structures and is characterized primarily by the streamwise component of vorticity. It is plausible that the peak in $E_{\omega x}$ may be associated with the ribs. Marasli et al. (1993) observed a peak at f_s in their ω_z-spectrum in a circular cylinder wake at x/d = 30 and Re = 2000, but not in their ω_x- or ω_y-spectrum. Zhou & Antonia (1993) reported that both the peak vorticity and circulation associated with spanwise structures decay exponentially as x/d increases from 10 to 60. Such a rapid decay should be associated with rapid weakening of vortex stretching that occurs between the successive spanwise structures. Since vortex stretching plays a key role in generating ribs (Hayakawa & Hussain, 1989), the strength of the ribs should decay rapidly as x/d increases. Consequently, the ω_x-spectrum may not show a peak at the shedding frequency at x/d = 30.

5. ANGLES OF THE VORTICITY VECTOR

The instantaneous angles of the vorticity vector may provide insight into the orientation of vortical structures. The angles are defined by

$$\alpha = \tan^{-1}(\omega_y / \omega_x), \tag{3a}$$

$$\beta = \tan^{-1}(\omega_z / \omega_x), \tag{3b}$$

$$\gamma = \tan^{-1}(\omega_z / \omega_y), \tag{3c}$$

Fig 4 shows the probability density function p of these angles for y ≥ 0. Above the centreline, $p(\alpha)$ (Fig 4a) shows a significant peak at $\alpha \approx 50°$, suggesting that vortical structures in the (x, y)-plane are most probably oriented at $\alpha \approx 50°$ to the x direction. The present observation is consistent with the notion that the longitudinal structures are approximately aligned with the diverging separatrix, whose inclination to the x-axis through the saddle point was found to be about 50° (Zhou & Antonia 1994). Bisset et al. (1990) also found a peak

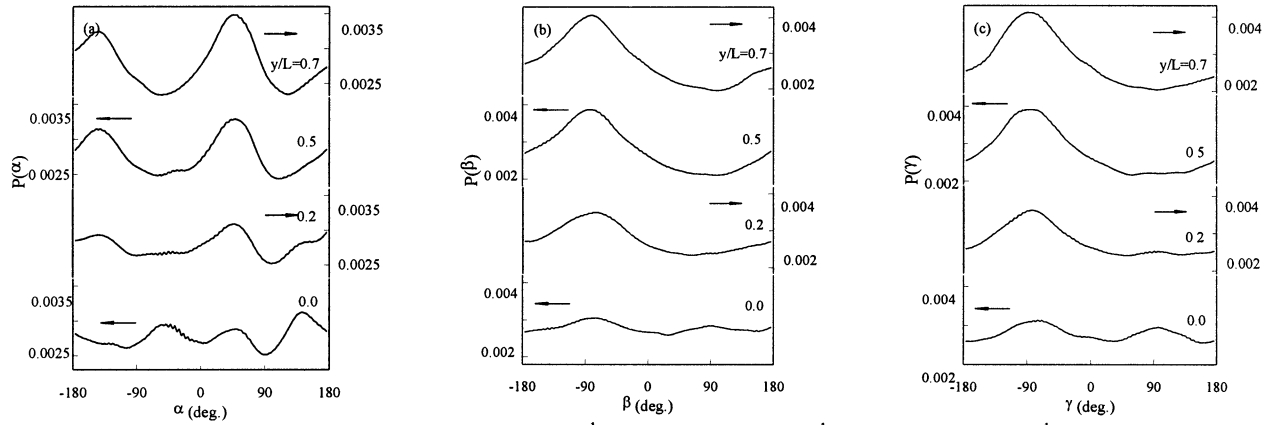

Figure 4 Probability density functions of (a) $\alpha = \tan^{-1}(\omega_y / \omega_x)$, (b) $\beta = \tan^{-1}(\omega_z / \omega_x)$, (c) $\gamma = \tan^{-1}(\omega_z / \omega_y)$

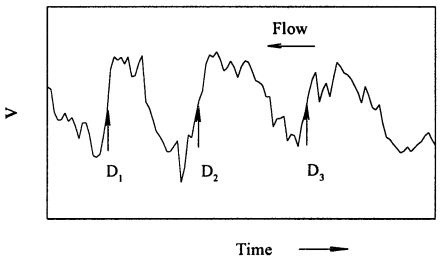

Figure 5 Trace of v and detections using the *WAG* technique (D_1, D_2 and D_3 denote downstream detections), y/L ≈ 0.5.

in $p\ (\alpha)$ at $\alpha \approx 45°$ in a turbulent far-wake, which is slightly different from the present observation. The difference may not be entirely due to the experimental uncertainty. The spanwise vortical structures in the near-wake have their origin in the vortex shedding process, while the dynamical process for the formation of far-wake vortical structures is likely to be more complicated. As a result, the behaviors between the two types of vortical structures are not the same (Zhou & Antonia 1995). Since vortex stretching plays a key role in generating ribs, one may surmise that the behaviors of ribs may be different between near- and far-wakes. The distribution of $p\ (\alpha)$ exhibits another peak at about -140°, a shift of about 180° from the other peak. Noting that ribs, aligned with the diverging separatrix, may have positive or negative ω_x and ω_y, the peak at -140° is simply the same consequence as that at 50° (Moin & Kim 1985; Bisset et al. 1990). The distributions of $p\ (\beta)$ (Fig 4b) and $p\ (\gamma)$ are quite similar, but they are different from $p(\alpha)$. There is no 180° period. A broad peak occurs at -90°, apparently due to predominantly negative spanwise vorticity associated with Karman vortices.

6. CONDITIONAL DATA

Detections of Spanwise Vortical Structures

Characteristic features of spanwise structures (e.g. a relatively sharp increase and decrease in u or v) were detected with the window average gradient (WAG) methods described in detail in Antonia and Fulachier (1989) and Bisset et al. (1990). Briefly, this scheme identifies a change (either an increase or decrease) in average signal level over a specified time interval. A computational window of length 2σ + 1 points (digital samples) is moved point by point through the data say v (t_I) (I = 1, 2, …, N, where N is the total number of data) and the value of WAG_j, where

$$WAG_j = \frac{sign}{2\sigma}\left(\sum_{i=j+1}^{j+\sigma} v(t_i) - \sum_{i=j-\sigma}^{j-1} v(t_i)\right)$$

$$j = \sigma + 1, \sigma + 2, \ldots, N\text{-}\sigma \qquad (4)$$

The value of *sign* is + 1 or – 1, and σ is set equal to about half the number of data points corresponding to the average spanwise structure period.

A detection region begins when WAG_j first exceeds $\kappa v'$, where κ is a threshold chosen such that the average detection frequency is approximately equal to the average spanwise structure period; it ends when WAG_j drops below zero. The detection instant j_m within each detection region is the value of j for which WAG_j is largest. This occurs at the downstream and upstream regions when *sign* is + 1 or – 1, respectively.

The *WAG* technique was applied to v (t_I). A total of about 2000 events were detected. Typical detections obtained for *sign* = + 1 are shown in Fig 5.

Conditional Average

The conditional average of an instantaneous quantity F is given by

$$< F >_k = \frac{1}{N}\sum_{m=1}^{N} F_{j_m + k} \qquad (5)$$

where k represents time (in samples, positive or negative) relative to the detection points j_m. (For convenience, the subscript τ will be omitted hereinafter.)

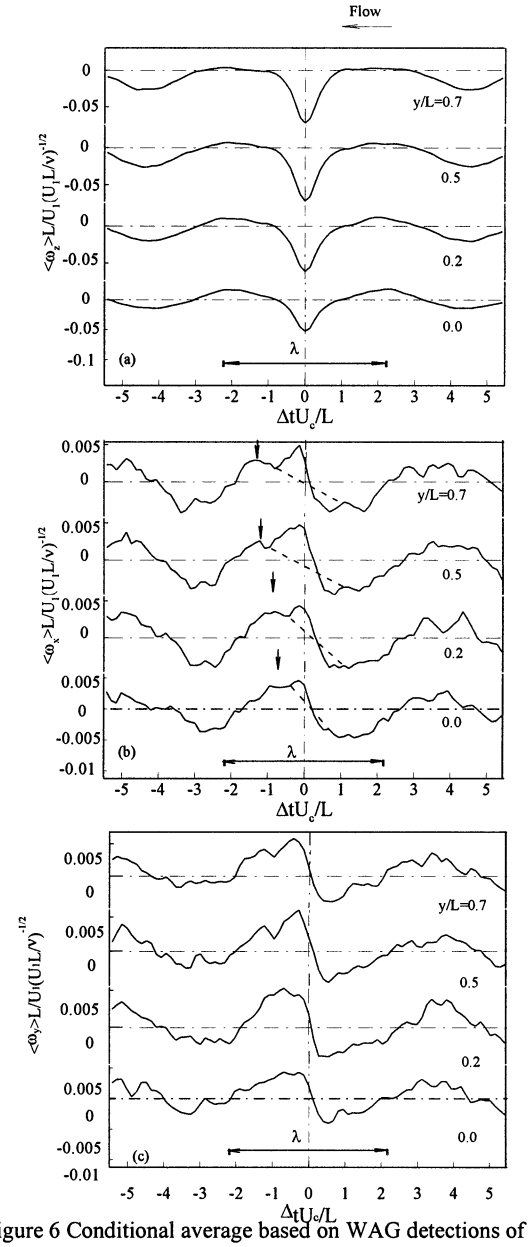

Figure 6 Conditional average based on WAG detections of the v signal (slope k =1): (a) $<\omega_z>$; (b) $<\omega_x>$; (c) $<\omega_y>$

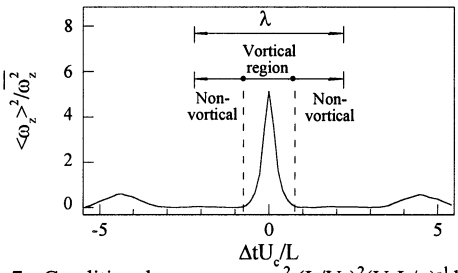

Figure 7 Conditional average $<\omega_z>^2 (L/U_1)^2(U_1L/v)^{-1}$ based on WAG detections of the v signal (slope k =1).

F can be viewed as the sum of the time mean component $\overline{F}$ and the fluctuation component f. The latter can be further decomposed into the coherent fluctuation $\tilde{f} \equiv \langle f \rangle$ and a remainder (incoherent fluctuation) f_r, viz.,

$$f = \tilde{f} + f_r \tag{6}$$

Also,

$$< fg >= \tilde{f}\tilde{g} + < f_r g_r > \tag{7}$$

where f and g can each stand for either ω_x, ω_y or ω_z.

Conditional vorticity

Fig 6 presents the conditionally averaged vorticity both on and above the centreline; λ indicates the average wavelength of the spanwise vortical structures. All three components appear periodical, indicating a wavelength of λ, which is consistent with the Strouhal number. A strong negative peak occurs in $<\omega_z>$ (Fig 6a) at the detection instant $\Delta tU_c/L = 0$, indicating that detections are quite reasonable. Peaks can also be observed in $<\omega_x>$ and $<\omega_y>$ near $\Delta tU_c/L = 0$. Since turbulent vortical structures are highly three-dimensional, it should not be surprising to see the relatively strong concentration of the streamwise and transverse vorticity components around the peak of the spanwise component. Note that another peak, as indicated by an arrow, is also identifiable in $<\omega_x>$. This peak appears approaching the detection instant as y/L approaches the centreline, consistent with the suggestion (Fig 5 in Hussain & Hayakawa 1987) that ribs are aligned with the diverging separatrix. The location of the peak also corroborates Zhou & Antonia (1994)'s observation that ribs occur upstream of the saddle point. It seems that the relatively strong concentrations of $<\omega_x>$ or $<\omega_y>$ partly results from the three-dimensionality of the spanwise tructures and partly from the longitudinal structures. A dashed line is drawn in Fig 6b to help distinguish between the two effects.

Structural Average

If the conditionally averaged structure begins k_1 samples before the detection instant and ends k_2 samples after this instant, a structural average is denoted by a double overbar, e.g.

$$< \overline{\overline{fg}} >= \frac{1}{k_1 + k_2 + 1} \sum_{-k_1}^{k_2} < fg > \tag{8}$$

The value of k_1 (= k_2) is 16 so that the duration ($k_1 + k_2 + 1$) approximately corresponds to the average period of the spanwise structures. The ratio of $\overline{\overline{\tilde{\beta}\tilde{\gamma}}}$ or $\overline{\overline{\tilde{\beta}_r\tilde{\gamma}_r}}$ to $\overline{\beta\gamma}$ provides a useful measure of the coherent or incoherent contribution to $\overline{\beta\gamma}$.

We may identify the vortical region of the flow by the criterion $<\omega_z>^2/\overline{\omega_z} > 0.03$ and the non-vortical saddle region by $<\omega_z>^2/\overline{\omega_z} < 0.03$, as shown in Fig 7. It is evident that the vortical region does not occupy the same amount of space as the non-vortical region. Contributions to vorticity from each region may be estimated by weighting structural averages in proportion to the longitudinal extent λ of each region, namely

$$\overline{\overline{< fg >_v}}^* = [\lambda_v / \lambda] \overline{\overline{< fg >_v}}, \tag{9a}$$

$$\overline{\overline{< fg >_n}}^* = [\lambda_n / \lambda] \overline{\overline{< fg >_n}}, \tag{9b}$$

where the asterisk denotes the contribution to vorticity from either region and the subscripts v and n refer to vortical and non-vortical regions respectively.

The value of $\overline{\overline{< fg >_{sum}}}^* = \overline{\overline{< fg >_v}}^* + \overline{\overline{< fg >_n}}^*$ (Figs 8 though 10) is approximately equal to $\overline{fg}$, the departure being within 10% of $\overline{fg}$. This suggests that, for vorticity at least, the combination of the selected vortical and non-vortical regions is representative of the flow. In neither region, do the streamwise and transverse vorticity components vary greatly with y, but the spanwise component exhibits significant variation. The non-vortical region contributes more to $\overline{\omega_x^2}$ and $\overline{\omega_y^2}$ than the vortical region; $\overline{\overline{<\omega_x^2>}}_n^* / \overline{\omega_x^2}$ and $\overline{\overline{<\omega_y^2>}}_n^* / \overline{\omega_y^2}$ (Fig 8a and b) are about 60%. On the other hand, the vortical region contributes 40% or so. Note that the coherent contribution (Fig 9a and b) to $\overline{\omega^2}$ is very small, less than 1%. Longitudinal structures may have vorticities of opposite sign. The positive and negative vorticities may have cancelled each other out during the conditional averaging based on detections of spanwise vortical structures, resulting in a negligible coherent contribution to $\overline{\omega_x^2}$ and $\overline{\omega_r^2}$. For the spanwise component, the vortical region is dominating, $\overline{\overline{<\omega_z^2>}}_v^* / \overline{\omega_z^2}$ (Fig 8c) being between 60 and 80 %. The coherent contribution (Fig 9c) is almost entirely from the vortical region. But the non-vortical region accounts for most of the incoherent vorticity (Fig 10c).

7. CONCLUSIONS

Longitudinal and spanwise structures in a turbulent near-wake (x/d = 20) have been investigated using simultaneously information on the likely spatial relationships between the two types of vortical structures. Both $<\omega_x>$ and $<\omega_y>$ exhibit concentrations near the detection of the spanwise structure and upstream of the saddle point. This is attributed to the three-dimensionality of the spanwise structures and the occurrence of ribs. The conditional distributions of ω_x and ω_y, and the phase angle between ω_x and ω_y measured (large-scale) approximations to the three vorticity components. The present measurements provide useful qualitative, indicate that the longitudinal vortical structures are located upstream of the saddle point. The most likely inclination, to the x-axis, of longitudinal structures is about 50°, aligned with the diverging separatrix between the consecutive spanwise structures. It appears that rib-like structures are closely associated with the spanwise vortices. This seems fully consistent with available

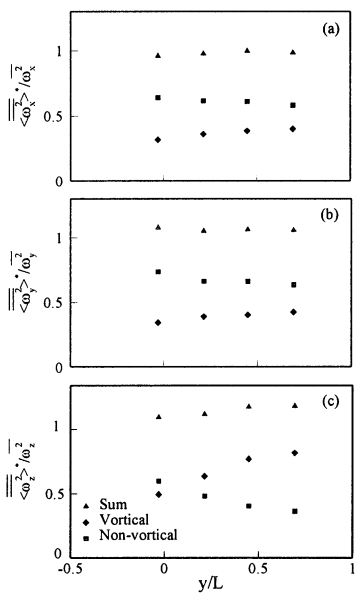

Figure 8 Lateral distribution of (a) $\overline{<\omega_x^2>}/\overline{\omega_x^2}$, (b) $\overline{<\omega_y^2>}/\overline{\omega_y^2}$, (c) $\overline{<\omega_z^2>}/\overline{\omega_z^2}$ for the vortical region (◆), non-vortical region (■) and their sum (▲).

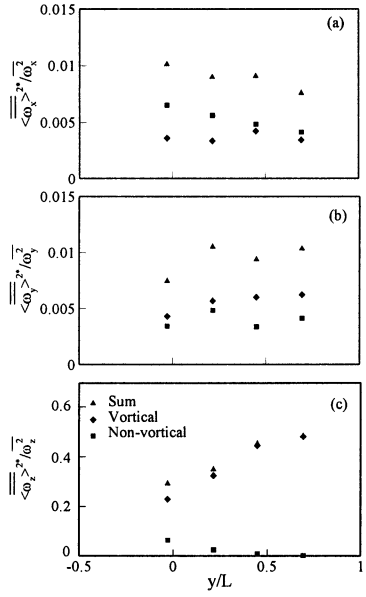

Figure 9 Lateral distribution of (a) $\overline{<\omega_x>^2}/\overline{\omega_x^2}$, (b) $\overline{<\omega_y>^2}/\overline{\omega_y^2}$, (c) $\overline{<\omega_z>^2}/\overline{\omega_z^2}$ for the vortical region (◆), non-vortical region (■) and their sum (▲).

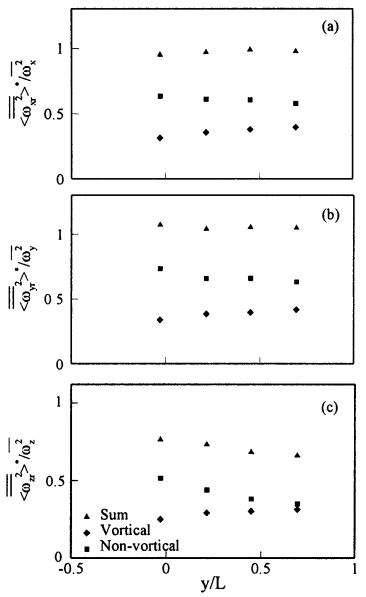

Figure 10 Lateral distribution of (a) $\overline{<\omega_{xr}^2>}/\overline{\omega_x^2}$, (b) $\overline{<\omega_{yr}^2>}/\overline{\omega_y^2}$, (c) $\overline{<\omega_{zr}^2>}/\overline{\omega_z^2}$ for the vortical region (◆),non-vortical region (■) and their sum (▲)

flow visualisations (e.g. Wu et al., 1994 and Elavarasan et al., 1998).

About 40% of variances $\overline{\omega_x^2}$ or $\overline{\omega_y^2}$ is associated with spanwise vortical structures, apparently resulting from the three-dimensionality of spanwise structures. The remaining 60% occurs in the non-vortical region, which may be largely attributed to longitudinal structures. The coherent contribution to $\overline{\omega_x^2}$ and $\overline{\omega_y^2}$, based on WAG detections, is negligibly small, probably due to cancellation of opposite-signed vorticities. About 60 to 80 % of $\overline{\omega_z^2}$ occurs within spanwise vortical structures. The coherent contribution to $\overline{\omega_z^2}$ is almost entirely from the vortical region, but the incoherent contribution is mainly from the non-vortical region.

ACKNOWLEDGMENTS

YZ wishes to acknowledge the financial support from the Research Grants Council of the Government of the HKSAR through Grant No. PolyU5161/97E. RAA is grateful for the continuing support of the Australian Research Council. Dr. J. Mi's contribution to the experimental work is much appreciated.

REFRENCES

Antonia, R.A. & Fulachier, L.: 1989. *J. Fluid Mech.*, **198**, 429-451.
Antonia, R.A., Rajagopalan, S. & Zhu, Y.: 1996a. *Expts. in Fluids*, **20**, 393-394.
Antonia, R.A., Zhu, Y. & Shafi, H.S.: 1996b. *J. Fluid Mech.*, **323**, 173-200.
Balint, J.-L., Wallace, J.M. & Vukoslavcevic, P.: 1989. *Advances in Turbulence II* (ed. H.H.Fernholz & H.E.Fiedler) pp.74-78. Springer.
Balint, J.-L., Wallace, J.M. & Vukoslavcevic, P.: 1991. *J. Fluid Mech.*, **228**, 53-86.
Bisset, D.K., Antonia, R.A. and Britz, D.: 1990. *J. Fluid Mech.*, **218**, 463-482.
Elavarasan, R., Djenidi, L. & Antonia, R.A.: 1998. *Ninth Int. Symp. on Applications of Laser Techniques to Fluid Mechanics*, Lisbon, Vol. I, 2.1.1-2.1.5.
Hussain, A.K.M.F. and Hayakawa, M.: 1987. *J. Fluid Mech.*, **180**, 193 -229.
Hayakawa, M. and Hussain, F.: 1989. *J.Fluid Mech.*, **206**, 375-404.
Kiya, M. & Matsumura, M.: 1988. *J.Fluid Mech.*, **190**, 343-356.
Lemonis, G.C.: 1995. PhD thesis, Swiss Federal Institute of Technology, Zurich.
Marasli, B., Nguyen, P. & Wallace, J.M.: 1993. *Expts. Fluids*, **15**, 209-218.
Meiburg, E. & Lasheras, J.C.: 1988. *J. Fluid Mech.*, **190**, 1.
Mi, J. & Antonia, R.A.: 1996. *Expts in Fluids*, 20, 383-392.
Moin, P. & Kim, J.: 1985. *J. Fluid Mech.* **155**, 441-464.
Sreenivasan, K.R.: 1995. In *Symposium on Developments in Fluid Dynamics and Aerospace Engineering*, S.M. Deshpande, A. Prabhu, K.R. Sreenivasan & P.R. Viswanath (eds.), Banganore, Interline publishers: 159-190.
Tsinober, A. Kit, E. & Dracos, T.: 1992. *J. Fluid Mech.*, **242**, 169-192.
Williamson, C.H.K.: 1988. *Phys. Fluids*, **31**, 3165.
Wu, J., Sheridan, J., Welsh, M.C., Hourigan, K &Thompson, M.: 1994. *Phys. Fluids*, **6**, 2883-2885.
Zhou, Y. & Antonia, R.A.: 1992. *Expts in Fluids*, **13**, 63-70.
Zhou, Y. & Antonia, R.A.: 1993. *J.Fluid Mech.*, **253**, 643-661.
Zhou, Y. & Antonia, R.A.: 1994. *J. Fluid Mech.*, **275**, 59-81.
Zhou, Y. & Antonia, R.A.: 1995. *Expts in Fluids*, **19**, 112-120.